



Harnessing the Ecofriendly Antifouling Potential of Agelasine Alkaloids Through MetaTox Analysis and Computational Studies

Walter Balansa^{1*}, Riyanti², Kirsten H. Balansa³, Novriyandi Hanif⁴

¹Departement of Fishery and Maritime Technology, Politeknik Negeri Nusa Utara, Tahuna, 95812, Indonesia

²Faculty of Fisheries and Marine Science, Jenderal Soedirman University, Purwokerto 53122, Indonesia.

³Department of Informatic Engineering, Faculty of Engineering, Sam Ratulangi University, Manado 95115, Indonesia

⁴Department of Chemistry, Faculty of Mathematics and Natural Sciences, IPB University, Bogor 16680, Indonesia.

ARTICLE INFO

Article history:

Received 31 July 2024

Revised 15 August 2024

Accepted 12 December 2024

Published online 01 February 2025

ABSTRACT

Agelasine alkaloids derived from marine sponges of the genus *Agelas* represent a promising source of antifouling compounds with potential economic and environmental benefits. Notably, agelasine D (**1**), agelamide D (**2**), *epi*-agelasine C (**3**) and agelasidine A (**4**) are known antifoulants. However, their ecotoxicological parameters remain unreported, raising concerns about their suitability as eco-friendly antifoulants. To address this, glucuronidated and sulfated metabolites were generated using MetaTox. Their binding affinities against acetylcholinesterase (AChE) were evaluated through molecular docking using PyRx, and ecotoxicological parameters were assessed using EPI Suite™. Compounds **1–4** exhibited strong AChE binding (−7.5 to −11.4 kcal/mol), surpassing those of AChE inhibitors such as synoxalidinones A (**5**) and C (**6**) and commercial antifoulants like seanine_211 (**7**) and irgarol-1501 (**8**). Furthermore, these compounds also displayed unfavorable toxicological profiles similar to commercial antifoulants, including high log *K_{ow}* (3.78 to 5.46), BCF (3.16 to 145), BAF (138.0 to 590), and Log *K_{oc}* (−0.15 to 2.18) values, with longer biotransformation half-lives (266 to 590 days), indicating potential environmental and health risks. In contrast, glucuronidated and sulfated derivatives particularly **1a**, **3a**, **3c-3d**, **4a** and **4b** demonstrated stronger AChE binding (−8.0 to −12.3 kcal/mol) and significantly improved toxicological profiles, including low log *K_{ow}* (−0.94 to 1.29), BCF (0.64 to 1.28), BAF (0.23 to 3.16), and shorter half-lives (0.01 to 0.17 days), with non-toxic and non-mutagenic properties. While their efficient synthesis and effectiveness in real-world applications remain to be tested, compounds **1a**, **3a** and **3b** represent promising eco-friendly antifouling candidates.

Copyright: © 2025 Balansa *et al.* This is an open-access article distributed under the terms of the [Creative Commons Attribution License](https://creativecommons.org/licenses/by/4.0/), which permits unrestricted use, distribution, and reproduction in any medium, provided the original author and source are credited.

Keywords: *Agelas*, antifoulant, Eco-friendly, Agelasine, MetaTox

Introduction

Marine fouling represents one of the greatest environmental and economic challenges in human history, severely affecting ships, mariculture facilities, and other marine economic structures¹. Following the bans on effective but toxic substances, such as tributyl tin²⁻³ and, more recently, copper-based antifouling agents^{4,5}, efforts have increasingly focused on the discovery of eco-friendly alternatives^{1,6-10}. This shift is evident in the rising number of publications worldwide, specifically a surge in antifouling research documented on platforms like Google Scholar¹¹.

Marine sponges of the genus *Agelas* have emerged as a promising source of antifouling compounds, with *epi*-agelasine C demonstrating potent effects against marine algae like *Ulva* sp.¹², agelasine D (**1**) and agelamide D (**2**)¹³ (previously named ageloxime D due to its misidentification as of a formamide for an oxime moiety¹⁴) proving effective against the larvae of the barnacle, *Balanus improvisus* and biofilm forming bacteria *Staphylococcus epidermidis*, respectively¹⁵.

*Corresponding author. E mail: walter.balansa@fulbrightmail.org

Tel: +62 853 9600 1695

Citation: Balansa W, Riyanti, Balansa KH, Hanif N. Harnessing the Ecofriendly Antifouling Potential of Agelasine Alkaloids Through MetaTox Analysis and Computational Studies. Trop J Nat Prod Res. 2025; 9(1): 329 – 340 <https://doi.org/10.26538/tjnpr/v9i1.42>

Official Journal of Natural Product Research Group, Faculty of Pharmacy, University of Benin, Benin City, Nigeria

A recent study emphasized the importance of specific functional groups in their antifouling activity, particularly the 9-*N*-methyladeninium moiety and decaline rings in agelasines, and the hypotaurocyamine in agelasidines, which influence both binding affinities and toxicological profile¹⁰. Notably, agelasines with the 9-*N*-methyladeninium moiety show stronger binding but higher toxicity than those with hypotaurocyamine, although the reasons for this disparity remain unclear¹⁰. Additionally, it is still unknown whether modifying the 9-*N*-methyladeninium moiety could improve or reduce both binding affinity and toxicity. Thus, as public awareness on the importance of environmentally friendly antifouling grows^{16,17} and antifouling regulations tighten¹⁸, addressing these knowledge gaps is critical for advancing research and discovering new eco-friendly antifouling agents.

To address the aforementioned gaps, there is a necessity to integrate computational and toxicological analyses into future investigations. Computational studies have revolutionized drug discovery¹⁹, contributing to breakthroughs in areas, such as cancer treatment^{20,21}, infectious diseases²², neurological disorders²³, and eco-friendly antifouling discovery²⁴⁻²⁶. In particular, MetaTox²⁷ analysis facilitates the discovery of various glucuronidates and sulfates from a range of natural products²⁸⁻²⁹. While both glucuronidated and sulfated products are known to have better pharmacological values, being safe and relatively inactive³⁰, mounting evidence reveals interesting bioactivities in glucuronidated and sulfated metabolites including but not limited to anticancer, ion-channel modulation, and anti-Alzheimer properties³¹⁻³⁶, motivating recent synthesis efforts^{31,37-39}. This suggests that generating such derivatives from antifouling compounds may provide insights into their bioactivity and cytotoxicity toward humans, non-target organisms as recently shown in anthraquinone derivatives⁴⁰. Yet, this analysis has

not been widely applied in eco-friendly antifouling research⁴⁰. Likewise, a predictive model and tool like the Estimation Program Interface (EPI Suite™)⁴¹ allows assessment of the ecological risks posed by certain chemicals on organisms and the environment, although it is rarely applied in antifouling research⁴².

This study aimed to evaluate the antifouling potential of both glucuronidated and sulfated derivatives generated from known agelasine antifouling compounds such as agelasine D, agelamide D, as *epi*-agelasine C and agelasidine A, using a combination of toxicity study using EPI Suite™, MetaTox analysis and computational study using PyRx and targeting acetylcholinesterase. Our findings give insight into the potential of the current combinatorial approach in discovering environmentally friendly antifouling candidates.

Materials and Methods

Molecular Docking

Protein preparation. The PDB file of the crystal structure of 6G1U at resolution 2.85 Å was retrieved from protein databank website at (<http://www.rcsb.org/pdb>). The file was uploaded to Discover Studio software, optimized by removing water and heteroatoms from and adding hydrogen to the protein, and was subsequently docked with PyRx⁴³.

Ligand preparation. The selected ligands agelasine D (**1**), agelamide D (**2**), *epi*-agelasine C (**3**), and agelasidine A (**4**) are known potent antifoulants that have inspired numerous synthetic efforts to discover more biologically active analogues⁴⁴. Despite their strong antifouling activity, many of these compounds including agelasines exhibit unfavorable toxicological properties¹⁰ highlighting the need to derivatize agelasine alkaloids to yield more eco-friendly antifoulants. These considerations served as the main criteria for selecting compounds **1-4**, along with their glucuronidated and sulfated derivatives, as the primary ligands for this study. The cdx files of the agelasine alkaloids and their analogues were drawn using ChemDraw 12.0. The files were uploaded to PyRx molecular docking software, minimized and converted to pdbqt file format before docking. Post-PyRx macromolecule ligand preparation, docking was then conducted by AutoDock Wizard in which the setup of AutoGrid contained the following dimensions (Angstrom): X = 65.6271, Y = 141.9604, Z = 111.6365.

Toxicity Analysis using EPI Suite™

The isomeric Simplified Molecular Input Line Entry System (SMILES) for *epi*-agelasine C, agelasine D and agelamide D were obtained and uploaded to EPI Suite software developed by the US Environmental Protection Agency's Office of Pollution Prevention and Toxics and Syracuse Research Corporation (SRC) to obtain Log K_{ow} (*n*-octanol/water partition coefficient), Log BAF (ratio of fish to water concentrations with dietary intake), Log BCF (ratio of fish to water concentrations with no dietary intake), Log K_{oc} (organic water to water partition coefficient) and Bioconcentration Half-Life^{45,46}

MetaTox Analysis

The cdx files of all ligands were individually uploaded to MetaTox webtool at <http://way2drug.com/mg>. By setting the cut-off probability activity (*Pa*) larger than probability inactive (*Pi*) (*Pa* > *Pi*), the webtool generated 30 metabolites from agelasine D, agelamide D, agelasidine A and *epi*-agelasine C through phase I and II reactions. The products from phase II reactions, specifically glucuronidation and sulfation, were further evaluated.

Toxicology Score

In this study, we slightly modified the ADMET score method as reported by Guan and co-workers⁴⁷ to evaluate toxicological endpoints, including the following: Log K_{ow}, Log K_{oc}, Log BCF/BAF (<https://www.epa.gov/tsca-screening-tools/download-epi-suite-estimation-program-interface-v411>), Ames toxicity, hepatotoxicity, *Tetrahyena pyriformis* toxicity, and minnow test results (<https://biosig.lab.uq.edu.au/pkcsnm/>). Each endpoint was converted to a

binary value (1 for beneficial, 0 for harmful) based on predefined thresholds (Log K_{ow} < 3.25 = 1, > 3.25 = 0; Log K_{oc} < 3 = 1, > 3 = 0; Log BCF < 3.25 = 1, > 3.25 = 0; Ames Toxicity: No = 1, Yes = 0; Hepatotoxicity: No = 1, Yes = 0; *T. Pyriformis* Toxicity < -0.5 = 1, > -0.5 = 0; Minnow Test < -0.3 = 0, > -0.3 = 1) (<http://lmmdd.ecust.edu.cn/admetar2/>). The total Toxicology Score for each compound was calculated by summing these binary values.

Statistical Analysis

The experiment included three replicates for each treatment. Due to the identical values observed across the replicates, the standard deviation was zero. We used Fisher's Exact Test to determine whether parent compounds significantly differ from their metabolites generated through MetaTox. This test was chosen because the similarity among the replicates, along with the small sample size, made it more suitable for analyzing categorical data in small sample sizes, providing a more accurate assessment of significance when expected frequencies are low⁴⁸. We created contingency tables to compare the beneficial and harmful scores of the parent molecules and their corresponding derivatives. Beneficial and harmful scores were assigned based on specific criteria related to their efficacy and safety profiles. The analysis was performed using GraphPad QuickCalcs (GraphPad Software, available at <https://www.graphpad.com/quickcalcs/contingency1/>).

Data Visualization

Toxicity data for each compound was compiled, and re-structured using the pandas library in Python to create a data frame suitable for visualization. A heatmap was then generated using the seaborn library to clearly distinguish between beneficial (blue) and harmful (red) factors. This visualization provided an overview of the toxicity profile for each compound, highlighting patterns and differences between parameters.

Results and Discussions

As previously noted in the introduction of this article, agelasine D (**1**), agelamide D (**2**) and *epi*-agelasine C (**3**) have been reported as potent antifouling agents against the marine alga, *Ulva* sp., and larvae of the *Balanus* sp.^{12,15}. Also, agelasine D and its formamide derivative, agelamide D, were reported to exhibit unique antifouling activities; furthermore, **1** solely inhibits the growth of antifouling bacteria, while **2** prevents biofilm formation¹³. Most known antifouling agelasines have not undergone toxicity evaluation. In contrast, this research focuses on assessing the toxicity of known agelasines with antifouling activity for the purpose of producing environmentally friendly metabolites of these compounds with MetaTox. By comparing the toxicological profiles of these metabolites with their parent molecules, this study offers new insights into the toxicity of known antifouling agents and their potential as eco-friendly antifouling solutions.

Molecular Docking

Molecular docking revealed that the four antifouling agelasines interacted with both similar and distinct binding sites or pockets of 6G1U (Figure 1). Specifically, agelasine D (**1**) and agelasidine A (**4**) bound to site 2 of chain A of 6G1U, while agelamide D (**2**) and *epi*-agelasine C (**3**) interacted with site 10 of chain A and site 3 of chain B, respectively (Figure 1). These results suggest that compounds **1**, **3**, and **4**, which differ in the 9-*N*-methyladeninium unit for **1** and **3** (red) and in the decaline system (blue) for **1** and **4**, interacted with different sites on the same target protein. Conversely, agelasidine A (**4**) and agelasine D (**1**) both bound to the same pocket of 6G1U, despite **4** featuring a hypotaurocyamine moiety (pink) and a long-chain terpenoid, while **1** contains a 9-*N*-methyladeninium and decaline system (Figure 1).

A closer look indicated that compounds **1-3** interacted with similar amino acid residues compared to compound **4** (Table 1). Featuring 9-*N*-methyladeninium or its derivative and decaline moieties, compounds **1-3** consistently interacted with Trp84, Trp279, and Phe330. In contrast, compound **4**, which bears hypotaurocyamine and a long terpene, showed interactions with Trp84, Phe330, and Tyr334. Notably, the decaline system and 9-*N*-methyladeninium functional group in

compounds **1-3** consistently bind to Trp279 and Trp84, respectively, while the hypotaurocyamine and long terpene moieties in compound **4** bind to Gln74 and Trp84, respectively. Trp84, Tyr130, Phe330, and Phe331 are part of the AChE anionic site, located at the entry of the active center gorge where allosteric activators and inhibitors overlap⁴⁹. In particular, Trp84 and Phe330 are believed to participate in electrostatic interactions with AChE via π -bonding lending strong potential binding affinities^{50,51} (Table 1). While agelasine D (**1**), oxo-agelamide D (**2**) and *epi*-agelasine C (**3**) all displayed strong binding affinities, ranging between -11.9 and -12.9 Kcal/mol, compound **4** showed a significantly weaker binding affinity of -7.5 Kcal/mol (Table 1).

The differences in binding affinities between agelasine D (**1**), agelamide D (**2**), *epi*-Agelasine C (**3**), and agelasidine A (**4**) can be attributed to several structural factors, including steric hindrance, charge distribution, hydrophilicity, and specific binding interactions. While all compounds (**1-4**), except Agelamide D (**2**), contain a primary amine—crucial for strong AChE binding, as seen with huperzine A⁵²—the bulkier guanidine and sulfate groups in agelasidine A (**4**) may create steric hindrance, limiting the interaction depth which leads to weaker affinity⁵³. In contrast, Agelasine D (**1**) interacts more effectively with key residues Trp84 and Trp279 due to its compact structure and hydrophobic decaline moiety, which enhances its stabilization in the enzyme's active site. The charge distribution in agelasidine A further complicates binding, as the negatively charged sulfate group disrupts its interaction with the hydrophobic pocket of AChE, whereas the 9-*N*-

methyladeninium moiety of agelasine D creates favorable contacts with Trp84. Additionally, the guanidine group in agelasidine A binds to Gln74, which is less crucial for AChE inhibition yielding reduced affinity. Thus, the differences in molecular architecture, steric effects, and charge distribution explain the stronger binding affinity among compounds **1-4**⁵³⁻⁵⁴.

These findings align with previous studies. For example, Trp84 is known to affect the biomolecular inhibition of alkaloids against acetylcholinesterase (AChE). Specifically, indole alkaloids bearing carbamates located closer to Trp84 exhibit strong biomolecular inhibition, and vice versa⁵⁵. This indicates that the stronger binding affinity observed for agelasine D (**1**), agelamide D (**2**), and *ent*-agelasine C (**3**) is likely due to the interactions between their methyladenine moiety and Trp84 compared to the interaction between the terpenoid part and Trp84 in agelasidine A (**4**) (Figure 2). Additionally, earlier studies showed that small molecules can bind to specific surface regions on their macromolecular targets by forming distinct binding sites or binding pockets (Figure 1)⁵⁶. Moreover, these results are supported by the fact that structural changes or modifications in ligands can result in distinct binding modes on the same protein. Malhotra et al. (2017)⁵⁶ found that in 14% of cases, chemical modifications altered the binding modes of related ligand pairs either by creating different binding sites or by forming stronger interactions in different binding sites through new substituents.

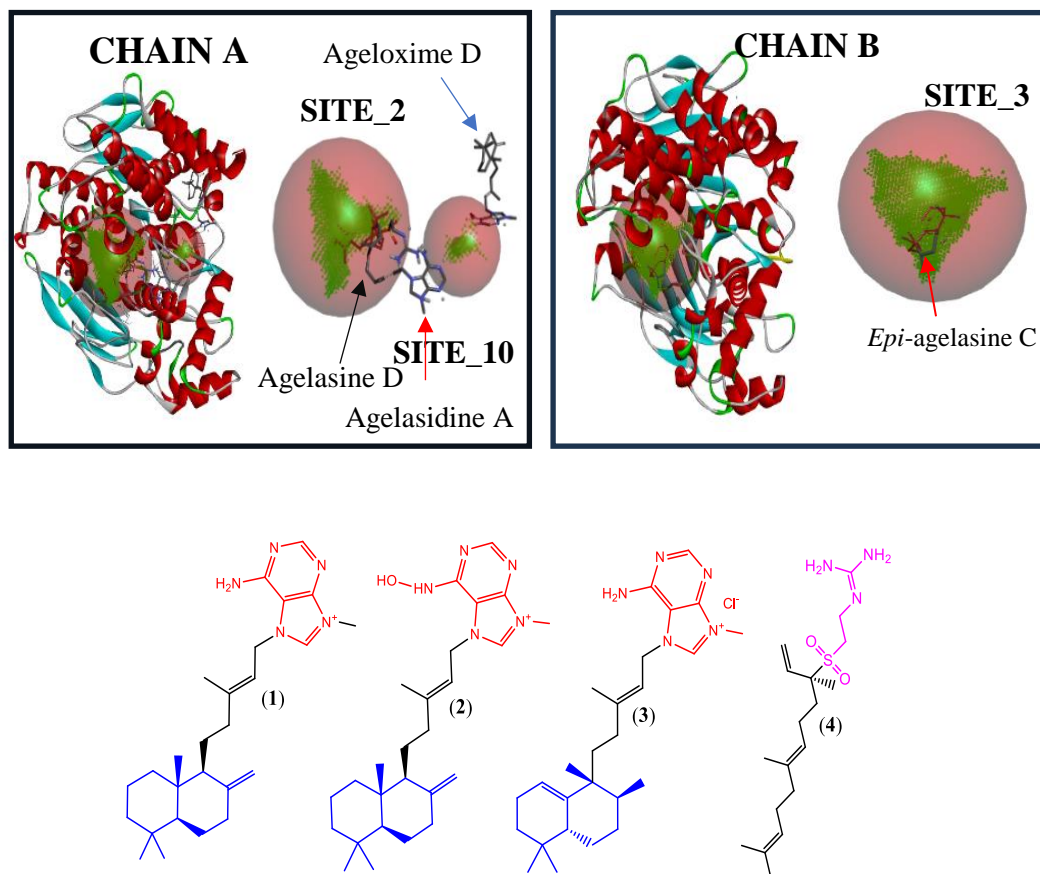


Figure 1: Bindings site of agelasine D, agelamide D, agelasidine A at chain A, *epi*-agelasine C at chain B of 6G1U (A) and their molecular structures (B).

Toxicity Study

To evaluate their potential as ecofriendly antifouling agents, the toxicity profiles of **1-4** were evaluated using environmental factors, such as Log K_{ow} , Log BCF, Log BAF, biotransformation half-life (BHL), and Log K_{oc} using EPI SuiteTM. Because the impact of these agents ranges in terms of trophic order, we measured several parameters, such as

hepatotoxicity, AMES toxicity, *T. pyriformis* toxicity, minnow test, and skin sensitization. Ligands with Log K_{ow} values ≥ 3.0 were classified as bioaccumulative, while ≤ 3.0 indicated non-bioaccumulative. Log K_{oc} values of ≥ 3.0 and ≥ 3.5 signified low bioaccumulation and medium adsorption, respectively. BAF/BCF values > 3.0 indicated high/moderate bioaccumulation, with persistence classified as rapid (\leq

1 day), moderate (1-30 days), or persistent (≥ 30 days). Water solubility was categorized as low (< 1 mg/mL), moderate (1-100 mg/mL), or high (> 100 mg/mL)⁵⁷⁻⁶⁵.

This analysis of agelasine D (**1**), *epi*-agelasine C (**2**), agelasidine A (**3**), and agelamide D (**4**) revealed that most compounds exhibited high toxicological parameters and hepatotoxic issues (Table 2). For instance, agelasine D, *epi*-agelasine C, agelasidine A, and agelamide D showed Log K_{ow} , Log BCF, Log BAF, and BHL values ranging from 3.23 to 5.48, 3.0 to 5.48, 3.16 to 145, and 1.08 to 50.40, respectively (Table 2). The majority of these values fall outside the thresholds for the corresponding parameters)⁵⁷⁻⁶⁵. These results suggest a high potential for bioaccumulation and indicate unfavorable toxicological parameters. Furthermore, with the exception of agelasidine A, all known antifouling agelasines (**1-3**) exhibited either hepatotoxicity, AMES toxicity, or both (Table 2), suggesting their potential to cause mutagenicity and hepatotoxicity in untargeted organisms. This necessitates the derivatization of these compounds to produce more favorable antifouling agents, potentially through MetaTox analysis³⁷⁻⁴⁰.

MetaTox and Ecotoxicological Analysis

By applying potential activity > 0.4 as cut off in a MetaTox analysis, we generated 13 metabolites particularly from phase II reaction, namely glucuronidation and sulfation. They include 1 sulfate (**1a**) and 3 glucuronides (**1b**, **1c**, **1d**) from agelasine D (**1**), 3 glucuronides (**2a**, **3a** and **4a**) from agelamide D (**2**), 1 sulfate (**3a**) and 3 glucuronides (**3b**, **3c** and **3d**) from *epi*-agelasine C (**3**) and 1 sulfate (**4a**) as well as 1 glucuronide (**4b**) from agelasidine A (**4**) (Figure 4).

The analysis also revealed glucuronidation and sulfation as the major products. Of the four parent molecules (**1**, **2**, **3** and **4**), a total of 10 metabolites (**1b**, **1c**, **1d**, **2a**, **2b**, **2c**, **3b**, **3c**, **3d** and **4b**) were generated mainly via *N*-glucuronidation reactions with N1, N3, N9 and the primary amine (NH₂), as well as the 9-*N*-methyladeninium moiety

contributing 3 metabolites (**1a**, **3a** and **4a**) (Figure 4). The attachment sites for glucuronidation occurred at either the amino or imine groups of the 9-*N*-methyladeninium in agelasines or NH₂ group at the hypotaurocyamine moiety in agelasidine, allowing the formation of ten glucuronidated products, which go as the following: metabolites **1b**, **1c** and **1d** from agelasidine D (**1**), **2a**, **2b** and **2c** from agelamide D (**2**), **3b**, **3c** and **3d** from *epi*-agelasine C (**3**), and **4b** from agelasidine A (Figure 4). These results indicate that the presence of the amino group in the 9-*N*-methyladeninium moiety seems to facilitate the sulfation reaction, while the replacement of the amino group with a nitroso derivative, such as in agelamide D (**2**) and its metabolites (**2b** and **2c**) did not. Replacement of the 9-*N*-methyladeninium moiety by a hypotaurocyamine in agelasidine A (**4**), led to the generation of two more metabolites, one sulfate (**4a**) and one glucuronide (**4b**).

Molecular docking of the glucuronidated and sulfated derivatives showed a slightly reduced binding energy between the derivatives and their corresponding parent molecules. For example, the sulfonated derivative (**1a**) showed a binding affinity of -12.1 Kcal/mol, which is similar to that of agelasine D (**1**) with a binding affinity of -12.1 Kcal/mol. The glucuronides derivatives (**1b**, **1c** and **1d**) showed slightly weaker binding affinities of -11.5 , -9.2 and -9.2 Kcal/mol, respectively. Similarly, agelamide D (**2**) showed binding affinities of -12.1 Kcal/mol while its glucuronidated analogues (**2a-2d**) showed slightly lower values of -10.4 , -9.9 , -11.4 Kcal/mol, respectively (Figure 4). Likewise, *epi*-agelasine C (**3**) exhibited a binding affinity of -11.8 Kcal/mol, which was slightly stronger than both its sulfate (**3a**) and glucuronide derivatives (**3b-3d**) with binding affinities of -9.0 , -9.7 , -10.1 and -9.7 Kcal/mol, respectively (Figure 3, Table 3). While all derivatives except **4a** exhibited slightly reduced binding affinities, most (excluding **4b**) still retained strong binding affinities towards the target receptor, with values below -8.0 kcal/mol (Figure 3).

Table 1: Docking score of agelasidine D, agelamide D, *epi*-agelasine C and agelasidine A against 6G1U target protein.

No	Ligands	Binding affinities (kcal/mol)	Amino acid residues
1	Agelasine D (1)	-13.2	His440 (hydrogen bond), Trp84, Phe330 (Electrostatic), Trp279, Phe330, His440, Trp84, Trp279, Phe330 (hydrophobic)
2	Agelamide D (2)	-12.1	Tyr334 (electrostatic), Try334, Trp84, Trp84, Trp279, Trp279 (hydrophobic)
3	<i>Epi</i> -agelasine C (3)	-11.8	Try334 (hydrogen bond), Trp84, Trp84, Phe330, Trp84, Trp84 (electrostatic), Phe330, Trp279, Phe330, Try334, Phe330, Try334, (hydrophobic)
4	Agelasidine A (4)	-7.50	Gln74 (hydrogen bond), Trp84, Phe330, Phe330, Phe330, Tyr334 (hydrophobic)

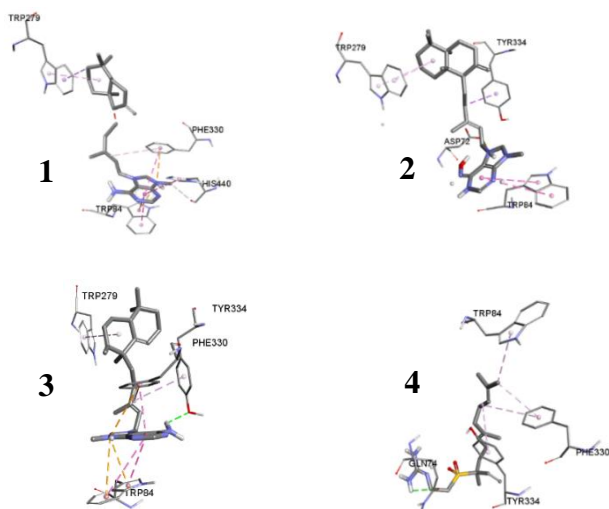


Figure 2: Molecular structures of agelasine D (**1**), agelamide D (**2**), *epi*-agelasine C (**3**) and agelasidine A (**4**).

Toxicological data analysis confirmed that all analogues exhibited relatively more favorable toxicological parameters. All analogues shared the same Log BCF value of 3.16, which was lower than that of the parent molecules (5-145), AChE inhibitors, and commercial antifoulants (5.16-109). Analogues **1a**, **1d**, **2a-2b**, **3a-3d**, and **4a-4b** showed low Log K_{ow} values ranging from -1.48 to 2.92, indicating low sorption potential⁶⁵. Except for **2a-2c**, the biological half-lives (BHL) of the remaining derivatives ranged from 0.09 to 1.41, suggesting a short half-life comparable to AChE inhibitors and commercial antifoulants, while surpassing their parent molecules (7.45–50.4). Except for analogues **2a-2d** and **3b**, the remaining derivatives displayed low bioaccumulation factor (BAF) values between 0.89 and 2.9, which were lower than those of the parent compounds (18.6-4150), AChE inhibitors (4.91–11.0), and commercial antifoulants (91.2–211). These findings suggest that analogues **1a**, **1d**, **3a**, **3c** and **3d** exhibited better toxicological values than compounds **1-8** (Table 4).

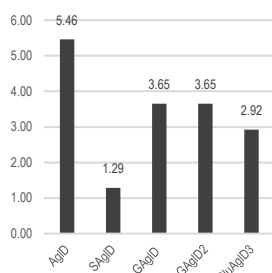
Water solubility and toxicological parameters varied among the derivatives. Compounds **1a-1d**, **2a-2c**, and **3a-3b** (0.45–65 mg/L) exhibited low to moderate solubility, contrasting with the significantly higher solubility (>100 mg/L) of **3c**, **3d**, **4a**, and **4d**⁶⁵. While high water solubility generally increases bioaccumulation potential in fatty tissues, low solubility favors sediment adsorption⁶⁵. However, the complex relationship between solubility and bioaccumulation also depends on hydrophobicity (Log K_{oc} , Log K_{ow} , etc.) of compounds. Low-solubility

compounds strongly bind to hydrophobic marine coatings, promoting sustained release. However, high Log K_{oc} and Log K_{ow} values increase bioaccumulation risk. Interestingly, compounds **1a**, **3a**, and **3b** displayed low Log K_{oc} (-0.94 to 1.283), Log K_{ow} (1.28–1.63) and BHL (<1 day) (Table 3), suggesting minimal bioaccumulation and strong

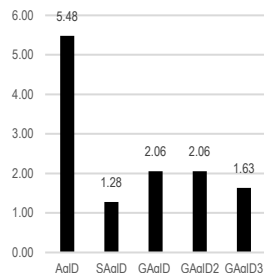
coating adhesion—essential antifouling characteristics.^{57,64} Their slow release resembles that of xanthone derivatives⁵⁷ but exceeds that of commercial antifoulants (**7-8**) with **7** and **8** exhibiting high values of Log K_{ow} > 3.59, BCF > 68.9 and BAF > 91.2 (Table 3)⁵⁷.

Table 2: Pharmacological parameters of agelasidine A, agelasidine D, agelamide D and *epi*-agelasine C evaluated using EPI-Suite™ and their general pharmacokinetic (Ames, hepatotoxic) evaluated using pkCSM.

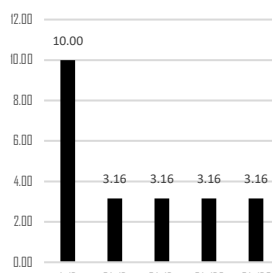
No	Compound	Log K_{ow}	Log BCF	BHL	Log BAF	Log K_{oc}	Ames Toxi-city	Hepato toxic	T. Pyriformi s toxicity	Min now Test	Skin
1	Agelasine D (1)	5.46	10.00	7.45	4150	5.48	No	Yes	0.285	-1.321	No
2	Agelamide D (2)	4.52	3.16	50.40	590.0	3.78	Yes	Yes	0.285	-0.097	No
3	<i>Epi</i> -agelasine C (3)	3.23	3.16	1.41	138.0	3.50	Yes	Yes	0.285	-0.256	No
4	Agelasidine A (4)	3.78	145.0	1.08	266.0	3.00	No	No	0.284	0.349	No
5	SynoxA (5)	2.05	10.5	0.244	11	1.95	Yes	No	0.285	0.816	No
6	SynoxC (6)	1.59	5.16	1.45	4.91	1.67	Yes	Yes	0.774	1.277	No
7	Seanine_211 (7)	3.59	109	1.03	211	2.88	No	No	2.63	-0.340	Yes
8	Irgarol_1501 (8)	2.77	14.6	0.257	17	2.63	No	Yes	0.387	0.610	No

Log K_{ow} (1a)

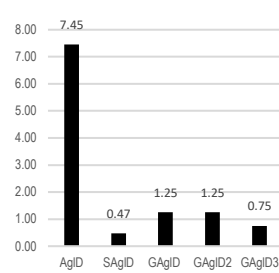
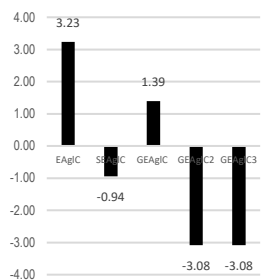
KocWin (1b)



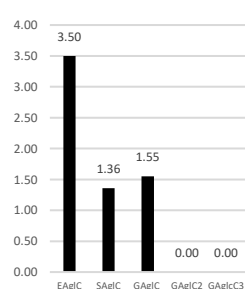
Log BCF (1c)



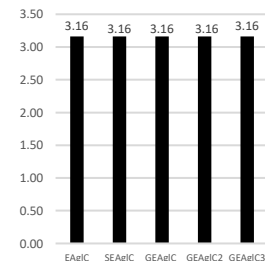
BHL (1d)

Log K_{ow} (2a)

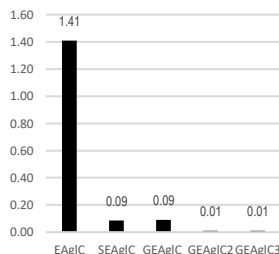
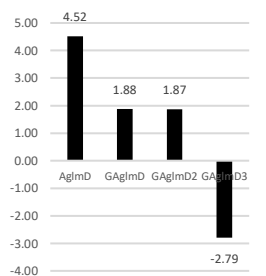
KocWin (2b)



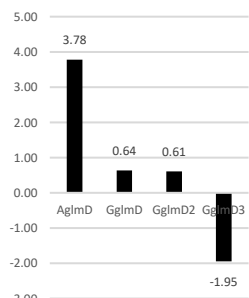
Log BCF (2c)



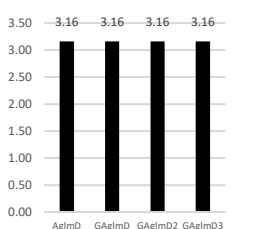
BHL (2d)

Log K_{ow} (3a)

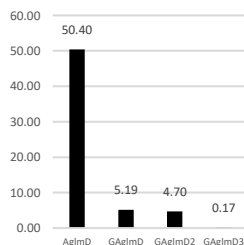
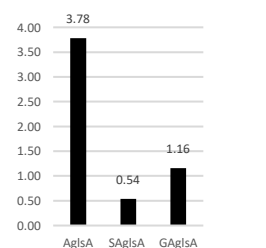
KocWin (3b)



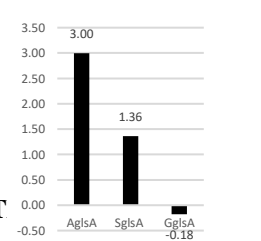
Log BCF (3c)



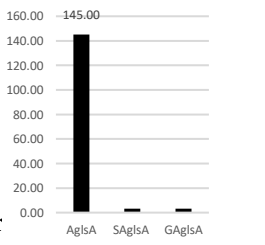
BHL (3d)

Log K_{ow} (4a)

KocWin (4b)



Log BCF (4c)



BHL (4d)

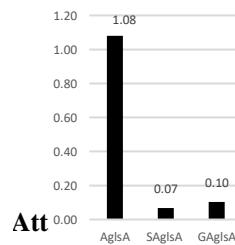


Figure 3: Toxicological data parameters for derivatives of agelasine D (**1a-1d**), agelamide D (**2a-2d**), *epi*-agelasine C (**3a-3d**), agelasidine A (**4a-4d**) obtained from EPI Suite™.**Table 3:** Toxicological parameters of agelasine D, *epi*-agelasine C, agelasine, agelamide D and their derivatives.

Compound	WS (mg/L)	Log K _{ow}	Log BCF	BHL	Log BAF	Log K _{oc}	hERG I/II Inh.	Ames	HPT	TPT	MT	SS
Agelasine D (1)	0.047	5.46	10.00	7.45	4150	5.48	N/Y	N	Y	0.285	-1.321	N
Sulf-agelasine D (1a)	0.535	1.29	3.16	0.47	2.9	1.28	N/N	N	N	0.285	-1.437	N
Glu-agelasine D (1b)	0.295	3.65	3.16	1.25	2.4	2.06	N/N	N	N	0.285	-0.061	N
Glu-agelasine D2 (1c)	0.295	3.65	3.16	1.25	2.4	2.06	N/N	N	Y	0.285	-0.198	N
Glu-agelasine D3 (1d)	1.283	2.92	3.16	0.75	68.8	1.63	N/N	N	Y	0.285	-0.487	N
Agelamide D (2)	194	4.52	3.16	50.40	590	3.78	N/Y	Y	Y	0.285	-0.595	N
Glu-agelamide D (2a)	1.423	2.64	3.16	8.06	46.5	1.06	N/N	N	Y	0.85	0.767	N
Glu-agelamide D2 (2b)	1.301	2.79	3.16	12.4	183	1.36	N/N	N	Y	0.285	-0.235	N
Glu-agelamide D3 (2c)	0.431	3.24	3.16	12.4	183	1.36	N/N	N	Y	0.285	-0.235	N
<i>Epi</i> -agelasine C (3)	2.310	3.23	3.16	1.41	138	3.50	N/Y	Y	Y	0.285	-0.256	N
Sulf- <i>epi</i> -agelasine C (3a)	25.68	-0.94	3.16	0.09	1.0	1.36	N/N	N	N	0.286	0.549	N
Glu- <i>epi</i> -agelasine C (3b)	2.65	2.29	3.16	0.44	18.6	1.28	N/N	N	Y	0.286	2.308	N
Glu- <i>epi</i> -agelasine C2 (3c)	4240	-1.48	3.16	0.03	0.89	-0.79	N/N	N	N	0.286	1.868	N
Glu- <i>epi</i> -agelasine C3 (3d)	4240	-1.48	3.16	0.03	0.89	-0.78	N/N	N	N	0.286	1.868	N
Agelasidine A (4)	3.383	3.78	145.0	1.08	266	3.00	N/Y	N	N	0.284	0.349	N
Sulf-agelasidine A (4a)	632.4	0.54	3.16	0.07	1.2	1.36	N/N	N	N	0.285	-0.097	N
Glu-agelasidine A (4b)	113.1	1.16	3.16	0.10	2.1	-0.18	N/N	N	N	0.285	1.174	N
SynoxA (5)	13.34	2.05	10.5	0.244	11	1.95	N/N	Y	Y	0.346	0.926	N
SynoxC (6)	34.35	1.59	5.16	1.45	4.91	1.67	N/Y	N	Y	0.306	1.921	N
Seanine_211 (7)	13.37	3.59	109	1.03	211	2.88	N/N	N	N	2.630	-0.344	Y
Irgarol_1501 (8)	7.517	4.07	68.9	0.23	91.2	2.63	N/N	N	Y	0.387	0.610	N

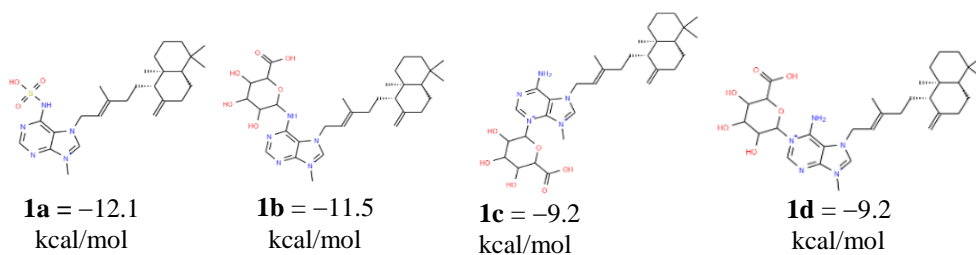
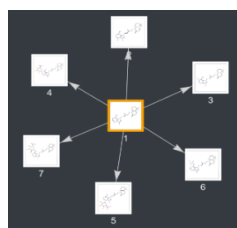
Note: WS (water solubility), hI (hERG Inhibitor), SS (skin sensitization), AMES (Ames toxicity), HPT (hepatotoxic), TPT (*T. pyriformis* toxicity), MT (Minnow toxicity).

We further performed toxicological scoring and statistical analysis to confirm the results. Adapting the ADMET score developed by Quan et al., 2019⁴⁷, we categorized the toxicological parameters and pharmacokinetic values of both parent and derivatives compounds into a binary system with 0 (red) representing harmful and 1 (blue), indicating beneficial properties (Table 4). The 13 endpoints (Log K_{ow}, Log BCF, BHL, BAF, Log K_{oc} etc.) of each derivative were tallied and divided by the total endpoints before being statistically compared to their parent molecules (Table 4).

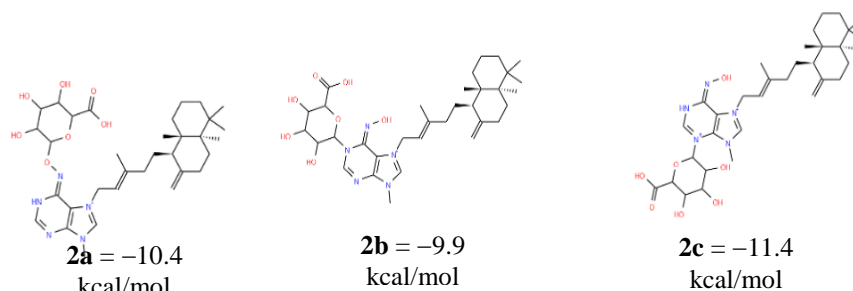
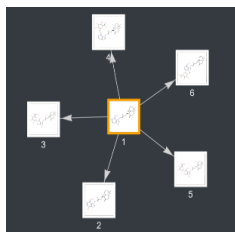
The scoring results indicate that all derivatives generally exhibited improved toxicological parameters compared to their parent molecules. For example, agelasine D (**1**) had a toxicological score of 0.30, while its derivatives (**1a-1d**) displayed higher scores of 0.85, 0.65, 0.65, and 0.65, respectively, although only agelasine D (**1**) and derivative 1a showed statistically significant differences ($p > 0.05$). Similarly, agelamide D (**2**) had a score of 0.30, while its derivatives (**2a-2c**) exhibited improved scores of 0.69, 0.69, and 0.62, though these differences were not statistically significant ($p > 0.05$). *Epi*-agelasine C (**3**) had a toxicological score of 0.38, significantly lower than its derivatives (**3a-3d**), which had scores of 0.92, 0.77, 0.85, and 0.85, respectively, with all analogues, except **3b**, showing statistically significant differences ($p > 0.05$). Agelasidine A (**4**) had the highest score among the parent molecules at 0.53, but its derivatives (**4a** and **4b**) exhibited much higher scores of 0.84 and 0.92, although these differences were not statistically significant ($p > 0.05$). Moreover, except for **2c**, the scores of all analogues (ranging from 0.69 to 0.92) were higher than those of synoxazolidinones A (**5**) and C (**6**), seanin_211 (**7**), and irgarol_1501 (**8**), which had scores ranging from 0.54 to 0.62, although these differences were not statistically significant

(Table 5). These findings highlight the trend that derivative compounds tend to have better toxicological profiles compared to both their parent molecules and some standard antifouling agents, as shown in Table 4 and Table 5.

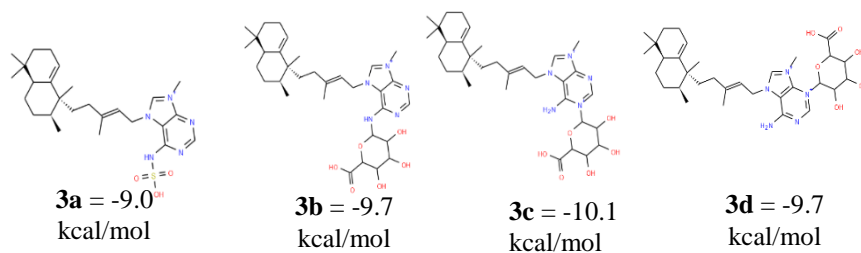
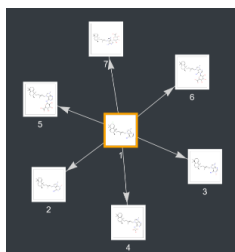
Equally important is that the derivatives also exhibited more favorable pharmacokinetic profiles compared to their parent molecules, AChE inhibitors, and commercial antifoulants. For instance, except for agelasidine A (**4**), the parent molecules (**1-3**) showed either hERG II inhibition, AMES mutagenicity, hepatotoxicity, or skin sensitization. Similarly, though to a lesser degree, synoxazolidinones (**5**, **6**), seanin_211 (**7**), and irgarol_1501 (**8**) also displayed issues such as AMES mutagenicity, hepatotoxicity, or skin sensitization (Table 3). In contrast, except for **2a-2d**, the remaining analogues did not show any concerns related to hERG inhibition, Ames mutagenicity, or hepatotoxicity. This suggests that the analogues, particularly **1a-1d**, **3a-3d**, and **4a-4b**, have fewer potential cardiac, hepatotoxic, and dermatological risks compared to the AChE inhibitors and commercial antifoulants. The results indicate the relevance of the present findings particularly for possible application of these compounds in mariculture industry where the use of such compounds as antifouling might be absorbed by cultivated organisms as shown in the accumulation of copper and zinc-based antifouling in sea bass and sea bream in the Mediterranean⁶⁶, posing a health risk to non-target organisms including human who consume such cultured marine organisms.



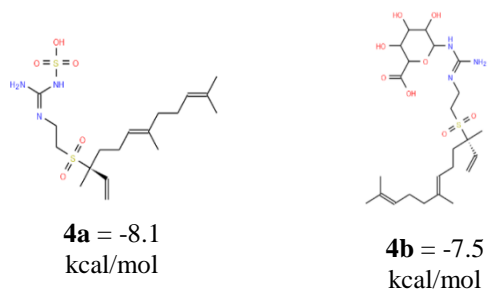
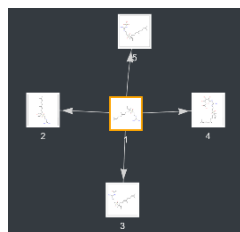
https://www.way2drug.com/metatox/view_path_smirks.php?id_task=666fa34369a0a&cut=0



https://www.way2drug.com/metatox/view_path_smirks.php?id_task=666fca446f547&cut=0.4

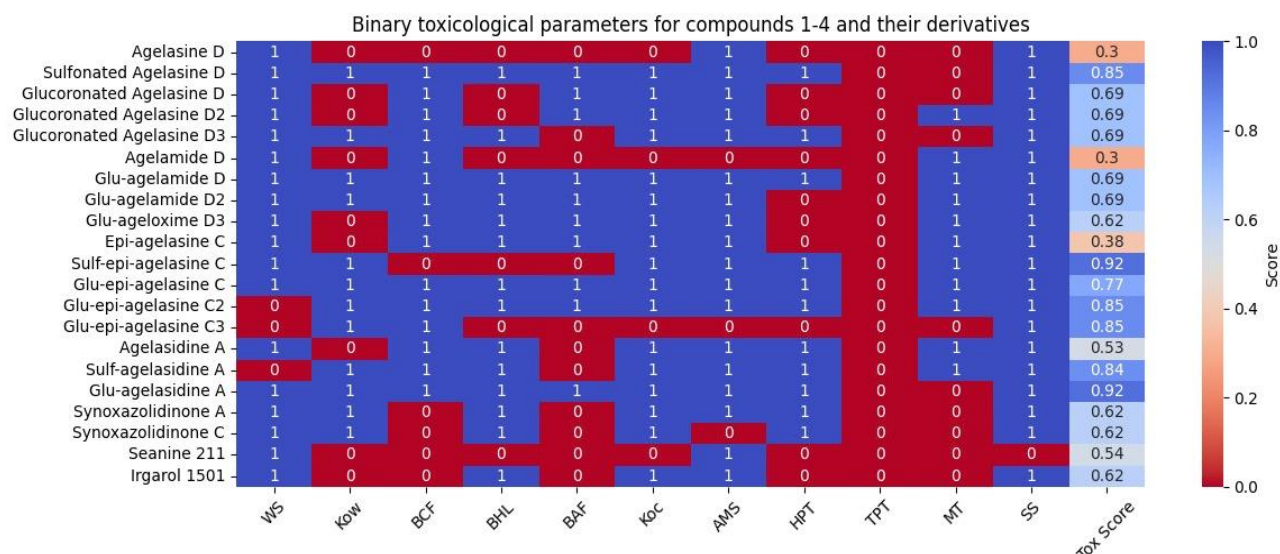


https://www.way2drug.com/metatox/view_path_smirks.php?id_task=666fc9875ed3d&cut=0



https://www.way2drug.com/metatox/view_path_smirks.php?id_task=666fd9706ce9e&cut=0

Figure 4: Molecular structures of agelasine D (1), agelamide D (2), *epi*-agelasine C (3) and agelasidine A (4) generated through MetaTox.



Note: WS (water solubility), hi (heRG Inhibitor), SS (skin sensitization), AMS (Ames toxicity), HPT (hepatotoxic), TPT (*T. pyriformis* toxicity), MT (Minnow toxicity). Green indicates useful, red harmful.

Figure 5: Binary toxicological parameters for agelasine antifouling agents and their derivatives

Table 4: 2x2 Contingency Table for agelasine D, agelasidine A, *epi*-agelasine C, ageloxime D and their derivatives

Comparison	Outcome 1	Outcome 2	Total	<i>p</i> value	Statistical significance
Agelasidine D (1)	4	8	13		
Sulf-agelasidine D (1a)	11	2	13	0.0154	**
Glu-agelasidine D (1b)	9	5	13	0.2377	*
Glu-agelasidine D2 (1c)	9	5	13	0.2377	*
Glu-agelasidine D3 (1d)	9	5	13	0.2377	*
Ageloxime D (2)	4	9	13		
Glu-ageloxime D (2a)	9	5	13	0.1152	*
Glu-ageloxime D2 (2b)	9	5	13	0.1152	*
Glu-ageloxime D3 (2c)	8	5	13	0.2377	*
<i>Epi</i> -agelasine C (3)	5	8	13		
Sulf- <i>epi</i> -agelasine C (3a)	12	1	13	0.0112	**
Glu- <i>epi</i> -agelasine C (3b)	10	3	13	0.1107	*
Glu- <i>epi</i> -agelasine C2 (3c)	11	2	13	0.0414	**
Glu- <i>epi</i> -agelasine C3 (3d)	11	2	13	0.0414	**
Agelasidine A (4)	7	6	13		
Sulf-agelasidine A (4a)	11	2	13	0.2016	*
Glu-agelasidine A (4b)	12	1	13	0.0730	*
Sulf- <i>epi</i> -agelasine C (3a)	12	1	13		
SinoxA (5) vs 3a	8	5	13	0.1602	*
SinoxC (6) vs 3a	8	5	13	0.1602	*
Seanin_211 (7) vs 3a	7	6	13	0.0730	*
Irgarol_1501 (8) vs 3a	8	5	13	0.1602	*

Note: * indicates not statistically significant, ** suggests statistically significant

These findings corroborate with studies showing that despite both being the most common phase II metabolic reactions³⁰, glucuronidation has a more prominent metabolic pathway than sulfation in many compounds. Firstly, conjugation reactions, catalyzed by uridine-5'-diphosphoglucuronosyltransferase (UGTs), such as glucuronidation are responsible for the metabolism of over 50% of the 200 most prescribed

drugs or approximately 12%⁶⁷ while sulfotransferases (SULTs), which catalyze sulfation reactions, contribute to the metabolism of 1%⁶⁸. Secondly, glucuronidation enzymes have more overlapping substrates and specificities compared to sulfation enzymes, allowing glucuronidation to metabolize a far greater number of compounds^{30,69}.

The discovery aligns with the report on sulfates and glucuronides. On the one hand, they are generally considered inactive and safe, with minimal impact on drug therapy^{30,71}. However, some metabolites produced by phase II conjugation, such as acyl glucuronides, sulfation metabolites, and glucuronides, can inhibit enzymes⁷¹ and modulate ion channel³². This inhibition can potentially affect drug efficacy and safety⁷¹. Similarly, while sulfation products are generally considered less toxic and deactivated, sulfated metabolites can also lead to the bioactivation of specific types of compounds, of which include benzylic and allylic alcohols, and aromatic hydroxylamines⁷². Hence, the discovery of **1a**, **3a** and **3b** corroborate with the discovery of active and strong glucuronidated and sulfated derivatives.

Thus, the application of MetaTox in generating agelasine analogues with reduced toxicity while maintaining high binding affinities indicates the potential of computational methods in facilitating the discovery of antifouling agents and other medically significant compounds⁷³. This discovery is particularly pertinent to current efforts in eco-friendly antifouling research⁷⁴, as the enhanced hydrophilicity and improved excretion profiles of glucuronidated and sulfated metabolites may lead to lower bioaccumulation and reduced toxicity. These advancements make them safer and potentially more effective for antifouling applications particularly in mariculture⁷⁵, aligning with the ongoing need for solutions that minimize environmental impact while ensuring efficacy.

This study also offers two significant benefits. Firstly, the combinatorial approach allows for the eco-friendly development of antifouling agents by revisiting known antifouling compounds such as agelasine D (**1**),

agelamide D (**2**), *epi*-agelasine C (**3**), and agelasidine A (**4**). This method is essential for advancing these compounds as antifouling agents while addressing the critical issue that has led to the banning of many environmentally harmful antifouling agents. By leveraging existing knowledge, this approach can potentially expedite the identification of safe and effective alternatives. This research also enhances our understanding of the non-cytotoxic properties of sulfated and glucuronidated agelasine alkaloids. Identifying non-cytotoxic compounds ensures that new antifouling agents will be both effective and environmentally safe, addressing a major concern associated with traditional antifouling practices in marine ecosystems.

Despite the significantly reduced pharmacological parameters in most derivatives, many still exhibit moderately higher BCF (3.16), BFA and hepatotoxic values indicating a need for further improvement. Additionally, further synthetic and field studies are essential for all derivatives identified here to support the development of environmentally friendly antifouling agents. Nevertheless, the present study provides valuable insights into the discovery of glucuronidated and sulfated agelasines as strong binders to acetylcholinesterase (AChE) with minimal environmental risk. These findings could pave the way for the development of effective, potent, and eco-friendly antifouling agents, contributing to the preservation of marine ecosystems.

Conclusion

In summary, following the toxicity evaluation of agelasine D (**1**), agelamide D (**2**), *epi*-agelasine C (**3**), and agelasidine A (**4**), 13 derivatives were generated through MetaTox analysis, primarily via glucuronidation and sulfation reactions. Subsequent molecular docking and toxicity studies revealed their strong binding affinity to 6G1U and improved toxicological parameters compared to their parent molecules particularly **1a**, **3a** and **3b**. These derivatives not only emerge as the most promising candidates for AChE inhibitors in this study, but also hold significant potential as eco-friendly antifouling agents. Their development represents a crucial step forward in the quest for sustainable and environmentally safe antifouling solutions, with promising implications for the preservation of marine ecosystems.

Conflict of Interest

The authors declare no conflict of interest

Authors' Declaration

The authors hereby declare that the work presented in this article is original and that any liability for claims relating to the content of this article will be borne by them

Acknowledgments

We thank Indonesian Higher Ministry of Education Funding for funding this research project (No. 79/SPK/D.D4/PPK.01.APVT/III/2024).

References

- Gomez, BJ. Marine natural products: a promising source of environmentally friendly antifouling agents for the maritime industries. *Front. Mar. Sci.* 2022;9:858757. doi.org/10.3389/fmars.2022.858757.
- Evans SM, Birchenough AC, Brancato MS. The TBT ban: out of the frying pan into the fire? *Mar. Poll. Bull.* 2000;40(3):204-211. doi.org/10.1016/S0025-326X(99)00248-9.
- Champ MA. A review of organotin regulatory strategies, pending actions, related costs and benefits. *Sci. Tot. Env.* 2000; 258(1-2):21-71. doi.org/10.1016/S0048-9697(00)00506-4.
- Blossom NW. Copper based antifouling—a regulatory update and recent scientific environmental studies. *Am. Chem. Corp.* 2014.
- Dafforn KA, Lewis JA, Johnston EL. Antifouling strategies: history and regulation, ecological impacts and mitigation. *Mar. Pollut. Bull.* 2011;62(3):453–465; doi: 10.1016/j.marpolbul.2011.01.012.
- Pan J, Xie Q, Chiang H, Peng Q, Qian PY, Ma C, Zhang G. “from the nature for the nature”: an eco-friendly antifouling coating consisting of poly(lactic acid)-based polyurethane and natural antifoulant. *ACS Sustain. Chem. Eng.* 2020;8(3):1671–1678. doi: 10.1021/acssuschemeng.9b06917.
- Liu LL, Wu CH, Qian PY. Marine natural products as antifouling molecules—a mini-review (2014–2020). *Biofouling* 2020;36(10):1210–1226. doi: 10.1080/08927014.2020.1864343.
- Qi SH, Ma X. Antifouling compounds from marine invertebrates. *Mar. Drugs* 2017;15(9). doi: 10.3390/md15090263.
- Wang KL, Wu ZH, Wang Y, Wang CY, Xu Y. Mini-review: antifouling natural products from marine microorganisms and their synthetic analogs. *Mar. Drugs* 2017;15(9). doi: 10.3390/md15090266.
- Balansa W, Riyanti, Manurung UN, Tomaso AM, Hanif N, Rieuwpassa, Schäberle TF. Sponge-based ecofriendly antifouling: field study on nets, molecular docking with agelasine alkaloids. *Trop. J. Nat. Prod. Res.* 2024;8(1):5913–5924. doi: 10.26538/tjnpr/v8i1.29.
- Jin H, Tian L, Bing W, Zhao J, Ren L. Bioinspired marine antifouling coatings: status, prospects, and future. *Prog. Mat. Sci.* 2022;124:100889. doi.org/10.1016/j.pmatsci.2021.100889.
- Hattori T, Adachi K, Shizuri Y. New agelasine compound from the marine sponge *Agelasma mauritiana* as an antifouling substance against macroalgae. *J. Nat. Prod.* 1997;60(4):411-3. doi.org/10.1021/np960745b.
- Hertiani T, Edrada-Ebel RA, Ortlepp S, van Soest RWM, de Voogd NJ, Wray V, Hentschel U. From anti-fouling to biofilm inhibition: new cytotoxic secondary

- metabolites from two Indonesian *Agelas* sponges. *Bioorg. Med. Chem.* 2010;18(3):1297–1311. doi: 10.1016/j.bmc.2009.12.028.
14. Paulsen B, Fredriksen KA, Petersen D, Maes L, Matheussen A, Naemi AO, Scheie AA, Simm R, Ma R, Wan B, Franzblau S. Synthesis and antimicrobial activities of N6-hydroxyagelasine analogs and revision of the structure of ageloximes. *Bioorg. Med. Chem.* 2019;27(4):620-9. doi.org/10.1016/j.bmc.2019.01.002.
 15. Sjögren M, Dahlström M, Hedner E, Jonsson PR, Anders V, Gunderson LL. Antifouling activity of the sponge metabolite agelasine D and synthesized analogs on *Balanus improvisus*. *Biofouling* 2008;24(4):251–258. doi: 10.1080/08927010802072753.
 16. Georgiades E, Kluz D, Bates T, Lubarsky K, Brunton J, Growcott A, Smith T, McDonald S, Gould B, Parker N, Bell A. Regulating vessel biofouling to support new Zealand's marine biosecurity system – a blue print for evidence-based decision making. *Front. Mar. Sci.* 2020;7. doi: 10.3389/fmars.2020.00390.
 17. Utama IKAP, Hermawan YA, Ariesta RC, Risdiyanto S, Sitingjak M, Ardhiyanto W. Protecting the Country from Bio-Invasion, a Case Study of Biofouling Management in Indonesia. In: IOP Conference Series: Earth Environ. Sci. Inst. Phys.; 2023. doi: 10.1088/1755-1315/1250/1/012022.
 18. Wang N, Zhang R, Liu K, Zhang Y, Shi X, Sand W, Hou B. Application of nanomaterials in Antifouling: A Review. *Nano Mat. Sci.* 2024. doi: 10.1016/j.nanoms.2024.01.009.
 19. Sabe VT, Ntombela T, Jhamba LA, Maguire GEM, Govender T, Naicker T, Kruger H. Current Trends in Computer Aided Drug Design and a Highlight of Drugs Discovered via Computational Techniques: A Review. *Eur. J. Med. Chem.* 2021;224. doi: 10.1016/j.ejmech.2021.113705.
 20. Shoaib TH, Ibraheem W, Abdelrahman M, et al. Exploring the potential of approved drugs for triple-negative breast cancer treatment by targeting casein kinase 2: Insights from computational studies. *PLoS One* 2023;18(8 August). doi: 10.1371/journal.pone.0289887.
 21. Ravnik Z, Muthiah I, Dhanaraj P. Computational studies on bacterial secondary metabolites against breast cancer. *J Biomol Struct Dyn* 2021;39(18):7056–7064. doi: 10.1080/07391102.2020.1805361.
 22. Jenner AL, Aogo RA, Davis CL, Smith AM, Craig M. Leveraging computational modeling to understand infectious diseases. *Curr. Pathobiol. Rep.* 2020;8(4):149–161; doi: 10.1007/s40139-020-00213-x.
 23. Monteiro AF, Viana JD, Nayarisseri A, Zondegoumba EN, Mendonça Junior FJ, Scotti MT, Scotti L. Computational studies applied to flavonoids against Alzheimer's and Parkinson's diseases. *Oxid. Med. Cell Longev.* 2018;2018. doi: 10.1155/2018/7912765.
 24. Gaudêncio SP, Pereira F. Predicting antifouling activity and acetylcholinesterase inhibition of marine-derived compounds using a computer-aided drug design approach. *Mar. Drugs* 2022;20(2). doi: 10.3390/md20020129.
 25. Arabshahi HJ, Trobec T, Foulon V, Hellio C, Frangež R, Sepčić K, Cahill P, Svenson J. Using virtual AChE homology screening to identify small molecules with the ability to inhibit marine biofouling. *Front. Mar. Sci.* 2021;8. doi: 10.3389/fmars.2021.762287.
 26. Almeida JR, Palmeira A, Campos A, Cunha I, Freitas M, Felpeto AB, Turkina MV, Vasconcelos V, Pinto M, Correia-da-Silva M, Sousa E. Structure-antifouling activity relationship and molecular targets of bio-inspired(thio)xanthenes. *Biomolecules* 2020;10(8):1–17. doi: 10.3390/biom10081126.
 27. Rudik AV, Bezhtsev VM, Dmitriev AV, Druzhilovskiy DS, Lagunin AA, Filimonov DA, Poroikov VV. MetaTox: Web application for predicting structure and toxicity of xenobiotics' metabolites. *J. Chem. Inf. Model.* 2017;57(4):638–642. doi: 10.1021/acs.jcim.6b00662.
 28. Marin DE, Taranu I. Using in silico approach for metabolomic and toxicity prediction of alternariol. *Toxins (Basel)* 2023;15(7). doi: 10.3390/toxins15070421.
 29. Agahi F, Juan C, Font G, Juan-García. In silico methods for metabolomic and toxicity prediction of zearalenone, α -zearalenone and β -zearalenone. *Food Chem. Toxicol.* 2020;146; doi: 10.1016/j.fct.2020.111818.
 30. Järvinen E, Deng F, Kiander W, Sinokki A, Kidron H, Sjöstedt N. The role of uptake and efflux transporters in the disposition of glucuronide and sulfate conjugates. *Front. Pharmacol.* 2022;12. doi: 10.3389/fphar.2021.802539.
 31. Docampo-Palacios ML, Alvarez-Hernández A, Adiji O, Gamiotea-Turro D, Valerino-Díaz AB, Viegas LP, Ndukwe IE, De Fátima Á, Heiss C, Azadi P, Pasinetti GM. Glucuronidation of methylated quercetin derivatives: chemical and biochemical approaches. *J Agr. Food Chem.* 2020;50:14790-807. doi: 10.1021/acs.jafc.0c04500.
 32. Vitku J, Hill M, Kolatorova L, Kubala Havrdova E, Kancheva R. Steroid sulfation in neurodegenerative diseases. *Front. Mol. Biosci.* 2022;9:839887. doi.org/10.3389/fmolb.2022.839887.
 33. Liang SC, Xia YL, Hou J, Ge GB, Zhang JW, He YQ, Wang JY, Qi XY, Yang L. Methylation, glucuronidation, and sulfonation of daphnetin in human hepatic preparations in vitro: metabolic profiling, pathway comparison, and bioactivity analysis. *J Pharm. Sci.* 2016;105(2):808-16. doi.org/10.1016/j.xphs.2015.10.010.
 34. Teles YC, Souza MS, Souza MD. Sulphated flavonoids: biosynthesis, structures, and biological activities. *Molecules.* 2018;23(2):480. doi.org/10.3390/molecules23020480.
 35. Williamson G, Kay CD, Crozier A. The bioavailability, transport, and bioactivity of dietary flavonoids: A review from a historical perspective. *Comp. Rev. Food Sci. Safety.* 2018;17(5):1054-112.
 36. Zheng J, Xiong H, Li Q, He L, Weng H, Ling W, Wang D. Protocatechuic acid from chicory is bioavailable and undergoes partial glucuronidation and sulfation in healthy humans. *Food Sci. Nut.* 2019;7(9):3071-80. doi.org/10.1002/fsn3.1168.
 37. Pranata A, Fitzgerald CC, Khymenets O, Westley E, Anderson NJ, Ma P, Pozo OJ, McLeod MD. Synthesis of steroid bisglucuronide and sulfate glucuronide reference materials: unearthing neglected treasures of steroid metabolism. *Steroids.* 2019;143:25-40. doi.org/10.1016/j.steroids.2018.11.017.
 38. Courtois A, Jourdes M, Dupin A, Lapèze C, Renouf E, Biais B, Teissedre PL, Mérillon JM, Richard T, Krisa S. In vitro glucuronidation and sulfation of ϵ -viniferin, a resveratrol dimer, in humans and rats. *Mol.* 2017;22(5):733. doi.org/10.3390/molecules22050733.
 39. Almeida AF, Santos CN, Ventura MR. Synthesis of new sulfated and glucuronidated metabolites of dietary phenolic compounds identified in human biological samples. *J Agri. Food Chem.* 2017;65(31):6460-6. doi.org/10.1021/acs.jafc.6b05629.
 40. Esmaeili SV, Alboghobeish A, Feyzi V, Ravannakhjavani F, Zendehtdel R. Virtual screening study for biological activity assessment and metabolism

- pathway of a fuel dye in airborne exposure scenario. *Tox. Ind. Health.* 2024;07482337241286187. doi.org/10.1177/07482337241286187.
41. Card, ML, Gomez AV, Lee WH, Lynch, DG, Orentas NS, Lee MT, Wong EM, Boethling RS. 2017. History of EPI Suite™ and future perspectives on chemical property estimation in US toxic substances control act new chemical risk assessments. *Env. Sci. Proc. Imp.* 19(3), pp.203-212.
 42. Vilas-Boas C, Silva ER, Resende D, Pereira B, Sousa G, Pinto M, Almeida J, Correia-da-Silva M, Sousa E. 3,4-Dioxygenated xanthenes as antifouling additives for marine coatings: in silico studies, seawater solubility, degradability, leaching, and antifouling performance. *Env. Sci. Poll. Res.* 2023;30(26):68987–68997. doi: 10.1007/s11356-023-26899-1.
 43. Dallakyan S, Olson AJ. Small-molecule library screening by docking with PyRx. *Chem. Biol. Meth. Prot.* 2015:243-50.
 44. Paulsen, B, Gundersen, L-L. The first synthesis of (–)-agelastine F; an antimycobacterial natural product found in marine sponges in the *Agelas* genus. *Eur. J. Org. Chem.*, 2020: 2244-2250. doi:10.1002/ejoc.202000202.
 45. Mackay D, Celsie AK, Powell DE, Parnis JM. Bioconcentration, bioaccumulation, biomagnification and trophic magnification: a modelling perspective. *Env. Sci. Proc. Imp.* 2018;20(1):72-85. doi: 10.1039/C7EM00485K.
 46. Canada justice law website. Persistence and bioaccumulation regulations SOR/2000-107 <https://laws-lois.justice.gc.ca/eng/regulations/sor-2000-107/page-1.html>.
 47. Guan L, Yang H, Cai Y, Sun L, Di P, Li W, Liu G, Tang Y. ADMET-score-a comprehensive scoring function for evaluation of chemical drug-likeness. *Medchemcomm* 2019;10(1):148–157. doi: 10.1039/C8MD00472B.
 48. Kim HY. Statistical notes for clinical researchers: Chi-squared test and Fisher's exact test. *Restor Dent Endod.* 2017 May;42(2):152-155. doi: 10.5395/rde.2017.42.2.152. Epub 2017 Mar 30.
 49. Bourne Y, Taylor P, Radić Z, Marchot P. Structural insights into ligand interactions at the acetylcholinesterase peripheral anionic site. *EMBO J.* 2003;22(1):1-12. doi: 10.1093/emboj/cdg005.
 50. Harel M, Quinn DM, Nair HK, Silman I, Sussman JL. The X-ray structure of a transition state analog complex reveals the molecular origins of the catalytic power and substrate specificity of acetylcholinesterase. *J Ame. Chem. Soc.* 1996;118(10):2340-6.
 51. Bajda M, Więckowska A, Hebda M, Guziar N, Sotriuffer CA, Malawska B. Structure-based search for new inhibitors of cholinesterase. *Inter. J Mol. Sci.* 2013;14(3):5608-32.
 52. Hansch C, Leo A, Taft RW. A survey of Hammett substituent constants and resonance and field parameters. *Chem. Rev.* 1991;91(2):165-95. doi.org/10.1021/cr00002a004.
 53. Sirimulla S, Bailey JB, Vegesna R, Narayan, M. Halogen interactions in protein-ligand complexes: implications of halogen bonding for rational drug design. *J Chem. Inf. Mod.* 2013; 53(11), 2781–2791. doi.org/10.1021/ci400257k.
 54. Pomponi M, Sacchi S, Colella A, Patamia M, Marta M. The role of TRP84 in catalytic power and the specificity of AChE. *Biophys. Chem.* 1998; 9:72(3):239-46. doi.org/10.1016/S0301-4622(98)00106-9.
 55. Govindaraj RG, Brylinski M. Comparative assessment of strategies to identify similar ligand-binding pockets in proteins. *BMC Bioinform.* 2018;19(1). doi: 10.1186/s12859-018-2109-2.
 56. Malhotra S, Karanicolas J. when does chemical elaboration induce a ligand to change its binding mode? *J. Med. Chem.* 2017;60(1):128–145. doi: 10.1021/acs.jmedchem.6b00725.
 57. Environment and climate change Canada (ECHA). Guidance on information requirements and chemical safety assessment. Environment and climate change Canada. 2017.
 58. Environment and climate change Canada (ECHA). Guidance on information requirements and chemical safety assessment. Environment and climate change Canada. 2021.
 59. Mackay D, Fraser A. 2000. Bioaccumulation of persistent organic chemicals: mechanisms and models. *Envion. Poll.* 110(3): 375-391. doi: 10.1016/S0269-7491(00)00162-7.
 60. Kobayashi Y. Analysis of the environmental parameters for risk assessment of pesticides by machine learning approach. Doctoral Thesis. 2021. University of Tsukuba, Japan
 61. Nikolaou M, Neofitou N, Skordas K, Castritsi-Catharios I, Tziantziou L. 2014. Fish farming and anti-fouling paints: a potential source of Cu and Zn in farmed fish. *Aquacult. Environ. Interact.* 5:163-171. doi: 10.3354/aei00101.
 62. Papa E, Sangion A, Arnot JA, Gramatica P. 2018. Development of human biotransformation QSARs and application for PBT assessment refinement. *Food Chem. Tox.* 112; 535–543. doi: 10.1016/j.fct.2017.04.016.
 63. Gimeno S, Allan D, Paul K, Remuzat P, Collard M. Are current regulatory log Kow cut-off values fit-for-purpose as a screening tool for bioaccumulation potential in aquatic organisms? *Reg. Tox. Pharmacol.* 2024;147:105556. doi.org/10.1016/j.yrtph.2023.105556.
 64. Gottardo S, Hartmann NB, Sokull-Klüttgen B. Review of available criteria for non-aquatic organisms within PBT/vPvB frameworks [Internet, November 19, 2024]. 2014.
 65. Vilas-Boas C, Neves AR, Carvalhal F, Pereira S, Calhorda MJ, Vasconcelos V, Pinto M, Sousa E, Almeida JR, Silva ER, Correia-da-Silva M. Multidimensional characterization of a new antifouling xanthone: structure-activity relationship, environmental compatibility, and immobilization in marine coatings. *Ecotox. Environ. Safety.* 2021; 228:112970. doi.org/10.1016/j.ecoenv.2021.112970.
 66. Nikolaou M, Neofitou N, Skordas K, Castritsi-Catharios I, Tziantziou L. Fish farming and anti-fouling paints: a potential source of Cu and Zn in farmed fish. *Aquaculture Environment Interactions.* 2014 18;5(2):163-71. doi: 10.3354/AEI00101.
 67. Guillemette C, Lévesque É, Rouleau M. Pharmacogenomics of human uridine diphosphoglucuronosyltransferases and clinical implications. *Clin. Pharmacol. Ther.* 2014;96(3):324–339. doi: 10.1038/clpt.2014.126.
 68. Cerny MA. Prevalence of non-cytochrome P450-mediated metabolism in food and drug administration-approved oral and intravenous drugs: 2006-2015. *Drug mpoMet. Disp.* 2016;44(8):1246–1252. doi: 10.1124/dmd.116.070763.
 69. P JanCova, M Siller. Topics on drug metabolism (Paxton J. ed). InTech. 2012. doi: 10.5772/1180.
 70. Pan LL, Yang Y, Hui M, Wang S, Li CY, Zhang H, Ding YH, Fu L, Diao XX, Zhong DF. Sulfation predominates the pharmacokinetics, metabolism, and excretion of forsythin in humans: major enzymes and

- transporters identified. *Acta Pharmacol. Sin.* 2021;42(2):311-22. doi: 10.1038/s41401-020-0481-8.
71. Tornio A, Filppula AM, Kailari O, Neuvonen M, Nyrönen TH, Tapaninen T, Neuvonen PJ, Niemi M, Backman JT. Glucuronidation converts clopidogrel to a strong time-dependent inhibitor of CYP2C8: a phase II metabolite as a perpetrator of drug–drug interactions. *Clin. Pharm. & Ther.* 2014;96(4):498-507. doi.org/10.1038/clpt.2014.141.
72. Yi L, Dratter J, Wang C, Tunge JA, Desaire H. Identification of sulfation sites of metabolites and prediction of the compounds' biological effects. *Anal. Bioanal. Chem.* 2006;386:666-74. doi: 10.1007/s00216-006-0495-1.
73. Ferreira LV, Santos TM, Tavares CA, Rasouli H, Ramalho TC. Atomistic origins of resurrection of aged acetylcholinesterase by quinone methide precursors. *Mol.* 2024;29(15):3684. doi.org/10.3390/molecules29153684.
74. Kyei SK, Darko G, Akaranta O. Chemistry and application of emerging ecofriendly antifouling paints: a review. *J Coat. Tech. Res.* 2020;17:315-32. doi.org/10.1007/s11998-019-00294-3.
75. Sen K, Erdogan UH, Cavas L. Prevention of biofouling on aquaculture nets with eco-friendly antifouling paint formulation. *Col. Techn.* 2020;136(2):120-9. doi.org/10.1111/cote.12454.